Energy & Environmental Science

Cite this: *Energy Environ. Sci.*, 2011, **4**, 965

www.rsc.org/ees

PAPER

High surface area templated $LiFePO_4$ from a single source precursor molecule†

Matthew R. Hill,*[abc] Gregory J. Wilson,[abc] Laure Bourgeois[d] and Anthony G. Pandolfo[abc]

Received 5th October 2010, Accepted 29th November 2010
DOI: 10.1039/c0ee00522c

The preparation of a stoichiometric dispersion of nanostructured $LiFePO_4$ clusters with intimate contact to carbon is described. This material exhibits outstanding performance for hybrid energy storage applications. A synthetic process, involving a novel single molecular source precursor, was developed and used to infiltrate a structured mesoporous carbon template. Subsequent optimisation of the infiltration process, reductive pyrolysis and secondary dispersion of the active materials for electrode coatings gave highly effective $LiFePO_4$/C composite electrodes suitable for high power applications. The materials were found to have surface areas in excess of 800 $m^2\ g^{-1}$ and TEM revealed an intimate contact to the carbon matrix as a result of the single source precursor employed. Extensive electrochemical performance evaluation, at rates exceeding 20 *C*, confirmed a resilient stable material capable of delivering exceptional high rate performance which is attributed to the periodic, interconnected mesopores (5–6 nm) and also the intimate $LiFePO_4$/C content delivered from the single source precursor. Galvanostatic charge–discharge cycling demonstrated the materials' excellent stability and high utilization, with a specific discharge capacity of 163 A h kg^{-1} (close to theoretical unity of 170 A h kg^{-1}) at 0.2 *C* and 128 A h kg^{-1} at 23 *C*, an exceptional result relative to lower surface area analogues. Power delivery was almost three times that of commercial $LiFePO_4$ at 10 *C*. These materials are well suited for application in high power energy storage devices including high power lithium batteries and hybrid devices.

Introduction

The viability and widespread use of renewable energy technologies, such as solar or wind power, are highly dependent on the development of improved electrochemical energy storage in order to offset the intermittent nature of these technologies. Ideally, the associated energy storage device must be able to quickly capture and release energy and to this end, energy storage materials that possess both high specific energy and power are highly sought after. Since the first reports detailing the preparation of olivine structured $LiFePO_4$ (also known as triphylite) from Goodenough *et al.*,[1] $LiFePO_4$ has been the subject of intense investigations with regard to its potential as an energy storage material. It is environmentally friendly, safe, has good

[a]*CSIRO Materials Science and Engineering, Private Bag 33, Clayton South MDC, Victoria, 3169, Australia. E-mail: Matthew.Hill@csiro.au*
[b]*School of Chemistry, University of Melbourne, Parkville, 3010, Australia*
[c]*CSIRO Energy Technology, PO Box 312, Clayton South, VIC, 3169, Australia*
[d]*Monash Centre for Electron Microscopy and Department of Materials Engineering, Monash University, Victoria, 3160, Australia*

† Electronic supplementary information (ESI) available: Detailed characterization data including mass spectra, X-ray diffraction patterns and scanning electron microscopy of prepared electrodes. See DOI: 10.1039/c0ee00522c

Broader context

Widespread usage of electrical storage materials depends upon improved charge and discharge times of storage materials. Here we present an approach that leads to a high surface area $LiFePO_4$ cathode material that has outstanding stability at fast charge/discharge rates, resulting in a power delivery 3 times that of a commercial material at 10 *C*. These remarkable results were achieved by using a novel single molecule precursor to $LiFePO_4$ that ensured phase purity within a nanoporous carbon matrix. These materials are well suited for application in high power energy storage devices including high power lithium batteries and hybrid devices.

thermal stability, is less costly than cobalt based materials and does not display the cyclability problems associated with $LiMn_2O_4$.[2,3] It has a theoretical specific capacity of about 170 A h kg^{-1} and because of the minimal changes in the unit cell parameters during the $LiFePO_4/FePO_4$ phase transition, the active material can be reversibly charged and discharged with a stable voltage profile at 3.45 V *vs.* Li^+/Li.[4,5] However, the low intrinsic electronic conductivity of this material and the slow diffusion of lithium ions across the two phase boundary seriously limit both the utilization and rate capability of the material.[1,3,5]

In order to improve the electrochemical properties of $LiFePO_4$ various strategies have been adopted in an attempt to improve the material including: controlling the size and crystallinity of the particles,[3,6,7] doping with supervalent cations (*e.g.* Nb^{5+})[8,9] or coating the material with a thin layer of conductive carbon.[10–12] Although in the case of supervalant cation doping, Herle *et al.* have demonstrated that the enhanced conductivity can be attributed to a percolating nano-network of metal-rich phosphides.[13] These strategies generally focus on improving the electrical conductivity of the bulk, or surface, of the material or on reducing the Li^+ diffusion distance by utilizing smaller, often nanosized, particles. Whilst many of these approaches have successfully improved the utilization capacity of $LiFePO_4$ at low discharge rates, the $LiFePO_4$ cathode still suffers from a rapid loss in capacity at increasing current density (*C*-rates).

Several research groups have demonstrated the improved performance of nanosized $LiFePO_4$ without the need for any surface treatment or carbon coating. Delacourt *et al.*[14] prepared ~140 nm sized $LiFePO_4$ by precipitation from water/DMSO, and when assembled into an electrode delivered a specific capacity of up to 147 mA h g^{-1} at 5 *C*-rate for thin film coatings. Similarly Lee *et al.*[15] produced 50–100 nm $LiFePO_4$ particles *via* a sol–gel method with a capacity of 150 mA h g^{-1}at 1 *C*-rate. However, in both studies, the specific capacity of the nanosized $LiFePO_4$ decreased rapidly at higher *C*-rates, typically to <100 mA h g^{-1} at *C*-rates >10–20 *C*. It is also worth noting that while these two nanosized materials were prepared without any *in situ* carbon coating, both studies utilized an *ex situ* conductive carbon black additive (up to 16.5%) in the preparation of their electrodes.

The majority of studies into high rate $LiFePO_4$ electrodes utilize some form of *in situ* carbon or carbon coating, in addition to particle size minimisation and the addition of *ex situ* conductive carbon, as this ensures intimate particle contact and optimal accessibility to the active material.[2,16–19] These methods generally rely on the formation of $LiFePO_4$ particles embedded in an amorphous carbon network derived from a carbon precursor. Specific capacities of typically ~150 to 160 mA h g^{-1} are achieved at *C*-rates <1 *C* whilst the capacities fall to ~120 to 125 mA h g^{-1} at 5 *C* and generally <100 mA h g^{-1} at higher rates (>10 *C*). Wang *et al.*[20] prepared 100 nm sized $LiFePO_4$ from a solid–liquid phase reaction and thermal decomposition, which gave an amorphous carbon coating, having a specific capacity of 167 mA h g^{-1} at 0.1 *C* and 122 mA h g^{-1} at 10 *C*. Cyclability for the composite material was reported, however only up to 10 *C* and at a very moderate charge rate (0.5 *C*), where the capacity was reasonably consistent for 50 cycles. These capacities are all generally higher than $LiFePO_4$–carbon composites prepared by ball milling/mixing with other conductive forms of carbon.[21,22] Recently Kang and Ceder[23] employed a ball milling approach to synthesize ~50 nm sized "off stoichiometric" $LiFePO_4$ material. When mixed with carbon black (15%) and formed into an electrode these particles delivered 166 mA h g^{-1} at 2 *C* and an astonishing ~135 mA h g^{-1} at 50 *C*. The same group also reported a similar electrode prepared with 65 wt% carbon black that had extremely high discharge rates of more that 100 mA h g^{-1} at 200 *C* and could still achieve 60 mA h g^{-1} at 400 *C*. Whilst the results of Kang and Ceder have generated considerable interest and debate, it should be highlighted such a material possessing high carbon loading is also likely to have a significant capacitive contribution from the porous carbon, which will be well suited to fast discharge rates.[24] In general, $LiFePO_4$ composites lead to enhanced utilisation of $LiFePO_4$ through improved ionic conductivity and in some cases increased surface area. However realisation of molecular scale $LiFePO_4$/C intimate mixing and order of magnitude increases in surface area remain vital for further exploitation of this effect.

It is evident that the electrochemical reactions in $LiFePO_4$ electrode materials rely upon lithium-ion (electrolyte) transport, which is a surface governed process; and therefore, the control and optimisation of the surface characteristics of such materials are crucial.[25,26] An approach for improving the performance of the material will be to increase its surface area, not only through a reduction in grain size, but also by an increase in porosity, as porosity and particle connectivity are known to be key factors to achieving high charge/discharge rate.[2,27]

The recent focus on developing cathodes with periodic mesoporosity is due to the delivery of a high surface area in conjunction with a stable, contiguous structure.[28] The high surface area ensures fast charge/discharge transfer at the electrode–electrolyte interface, and the contiguous structure ensures the stability of this performance over many cycles. These topologies are commonly approached through soft templating techniques,[29,30] yet with $LiFePO_4$ this approach has been restricted to mainly macroporous topologies with surface areas ~90 m^2 g^{-1},[1,25,31] although higher surface area Fe^{3+} based materials such as $Fe_3(PO_4)_3$[32,33] and $Li_3Fe_2(PO_4)_3$[34] are known. The high crystallisation temperature (*ca.* 750 °C)[35] required for $LiFePO_4$ generally precludes the use of a soft template based approach. Hard templates, such as periodic mesoporous carbons and silicas,[36–38] offer more stability at these temperatures, yet the challenges of infiltrating their fine pores with complex precursor mixtures in stoichiometric ratios, their subsequent condensation into the desired phase, and finally, template removal remain.

Herein we report the synthesis of $LiFePO_4$/carbon composites with exceptional surface area and ordered porosity. This class of materials are well suited to hybrid energy storage applications where high rate performance is key. The challenge of creating such a material means that novel precursors[39] and processing procedures are required. To this end we have developed a stratagem comprising: the use of a single molecular source for $LiFePO_4$, its subsequent infiltration within an ordered mesoporous carbon template, and a facile means for template removal through reduction. The precursor is soluble in aqueous based environments, allowing for stoichiometric ratios of Li, Fe and P to be readily infiltrated into the pores of a nanostructured carbon template. Preliminary electrochemical testing of the mesoporous $LiFePO_4$/carbon composites indicates exceptional performance at high discharge rates of up to 128 mA h g^{-1} at 23 *C*.

Experimental

A systematic series of nanostructured $LiFePO_4$ materials have been prepared *via* the use of a single molecular source infiltrated within an ordered mesoporous carbon, and structurally characterised with techniques including X-ray Diffraction (XRD), scanning electron microscopy (SEM), nitrogen adsorption and mass spectrometry (MS).

Equipment

X-Ray diffraction was performed on the powder diffraction beamline at the Australian Synchrotron with an incident wavelength of 1.00 Å. Each sample was placed in a 0.3 mm diameter quartz capillary and examined over the range of $2 < 2\theta < 82$. Analyses were performed on the collected XRD data for each sample with the Bruker XRD search match program EVA™. Crystalline phases were identified with the ICDD-JCPDS powder diffraction database. Surface areas were obtained on a Micromeritics ASAP 2400 surface area analyser. Samples were dried, degassed under vacuum and analysed *via* multi-point isothermal N_2 adsorption at 77 K using the BET method. Scanning electron microscopy was performed using a tungsten filament Leica S440 at a working distance of 25 mm with a probe current of 0.1 nA for secondary electron images and 2.0 nA for backscattered images, and an analysis chamber pressure of 1.0×10^{-7} Torr. Mass spectra were obtained on a VG Platform Quadrupole Mass Spectrometer employed in electrospray mode (ESI), with 3.0 kV capillary voltage and a cone voltage of 50 V in 100% MeOH eluent. The transmission electron microscopy (TEM) was conducted on a JEOL 2100F microscope operated at 200 kV and equipped with a JEOL energy dispersive X-ray (EDX) detector. The TEM images and diffraction patterns were recorded on a Gatan UltraScan CCD camera and electron-sensitive film, respectively. The EDX analysis was performed in scanning (S)TEM mode using a 0.7 nm probe. The EDX maps and high-angle annular dark field (HAADF)-STEM images for a given sample region were 256×256 pixels in size. The material was prepared for TEM observation simply by dispersing its powder form in high-purity ethanol and depositing a drop of the suspension onto a copper grid coated with holey-carbon film.

Methods: precursor LFP-S

In a typical synthetic procedure, 63% aqueous etidronic acid (5 mL, 1.52×10^{-2} mol) was added to 30 mL water and $LiOH \cdot H_2O$ (1.28 g, 3.05×10^{-2} mol) was added slowly to the mixture heated up to 80 °C. A white precipitate formed which eventually redissolved. Fresh $Fe(NO_3)_3 \cdot 9H_2O$ (12.36 g, 3.05×10^{-2} mol) was subsequently added portion-wise to the mixture, and following its dissolution, three equivalents of ethylene glycol (2.83 g, 4.56×10^{-2} mol) were added. The yellow-brown solution was heated overnight at 80 °C to remove water, yielding a yellow tar. This tar was then slowly heated under vacuum to a maximum of 140 °C over the course of eight hours, being maintained at this temperature for a further three hours. This vacuum decomposition of nitrates within the mixture is potentially explosive and must be carried out very slowly to ensure a controlled rate of decomposition. Yield 11.92 g of a free flowing light brown solid, precursor **LFP-S**. 1.00 g of this solid was then dissolved in 10 mL water, requiring lengthy sonication to achieve complete dissolution. Insoluble residues were separated *via* centrifugation. The solution was then added to 1.00 g of cubic mesoporous KIT-6 carbon,[40,41] and 5 drops of ethanol were added to improve wettability. The solvent was then evaporated overnight at 50 °C to give a black powder. This powder was heated under a flowing atmosphere of 5% H_2/95% N_2 at 1 °C min^{-1} to 750 °C and maintained at this temperature for ten hours to yield a black powder.

Electrochemical measurements

Coin cells (CR2032, Hohsen Japan) were assembled in a two electrode configuration in an Argon filled glove box where the cathodic (charging) electrode was 15.2 mm in diameter (1.81 cm^2) and the anodic electrode was 13 mm in diameter (1.33 cm^2). Electrode coatings were prepared by stirring and then ball milling a dispersion of 10% w/w binder (carboxy-methyl-cellulose, Sigma-Aldrich), with the powdered sample in water. Due to the low carbon content of sample 1 and the commercial sample, 20% w/w carbon black (SuperP, Timcal) was added to these electrode mixtures. The mix was then coated onto clean 30 μm aluminium foil, with a 60 μm calibrated grooved rod. Electrode loadings were expressed as the mass of the active material (m_{act}) per geometric area of the electrode. The anode was a lithium metal disk (300 μm, 99.99% purity, Sigma-Aldrich) electrically isolated from the cathode by a 25 μm polypropylene separator with 1 M $LiPF_6$ (50 : 50 w/w ethylene carbonate (EC) : dimethyl carbonate (DMC)) as the electrolyte (Mitsubishi Corp. Japan). Charge/discharge performance was evaluated on a series 4000 Maccor battery tester (Maccor, USA) under a constant current density equivalent to 0.2–23 *C* between 2.2 and 4.0 V *versus* Li/Li^+. A formation charge was first performed on the uncycled cells with constant current charge at 0.15 *C* to 4.0 V, potentiostatically held at 4.0 V until $I < C/24$, then discharged at 0.2 *C* for 2 cycles, then constant current at 0.3 *C* to 4.0 V, potentiostatically held at 4.0 V until $I < C/24$, then discharged at 0.1 *C* for a further 3 cycles. Cyclic voltammetry measurements were performed on a Voltalab Model PST050 Analytical Potentiostat (Radiometer), between 2.0 and 4.5 V *versus* Li/Li^+ in a two-electrode CR 2032 coin cell as described above with 1 M $LiPF_6$ (50 : 50 w/w ethylene carbonate (EC) : dimethyl carbonate (DMC)) as the electrolyte (Mitsubishi Corp. Japan).

Results and discussion

Despite the obvious utility of a periodic mesoporous $LiFePO_4$ morphology, to date there have been no reports of its successful generation, presumably due to the numerous synthetic challenges that need to be overcome. Amongst these challenges is the need to infiltrate soluble precursors in stoichiometric quantities within the confined spaces of a mesoporous template. To this end we have developed a novel chelating diyldiphosphonate double salt from a 1 : 2 stoichiometric compounding of 1-hydroxyethane-1,1-diyldiphosphonic acid (etidronic acid, EA) and the ubiquitous ethane-1,2-diol (ethylene glycol, EG). Prepared in careful stoichiometry with Li, Fe, and P, the combination results in a highly soluble aqueous precursor, $Li_2Fe_2(OH)_2(EA)(EG)_2$, represented in Fig. 1a.

Mass spectrometry (see Fig. S1, ESI†) confirms that the precursor preferentially forms a di-adduct with ethylene glycol. Moreover, the direct coordination of ethylene glycol to the $LiFePO_4$ precursor provides a carbon source that is intimately mixed with the active material. This soluble Li–Fe–P complex, herein referred to as the precursor **LFP-S**, allows for template infiltration *via* conventional solvent evaporation techniques and subsequent template removal according to Fig. 1b.

Table 1 summarizes the samples and preparation conditions for the $LiFePO_4$ materials examined in this study. Whilst the $LiFePO_4$ system benefits from the addition of a carbon precursor to improve conductivity, the attainment of intimate mixing can be problematic. Variations of the content of ethylene glycol often resulted in the introduction of impurity phases, $Li_4P_2O_7$ or $Fe_2P_2O_7$, most likely as the change in the additive ratio altered the double salt structure delivering insoluble oligomeric secondary phases. Ultimately, centrifugation of the aqueous solution of the double salt **LFP-S** followed by calcination under reducing atmosphere at 750 °C gave a phase pure mesoporous $LiFePO_4$ sample (Fig. 2).

Nanostructuring of the $LiFePO_4$ generated from this system was achieved *via* **LFP-S** infiltration into a cubic mesoporous KIT-6 carbon template.[41] Addition of small quantities of ethanol to an aqueous, centrifuged solution of the single source precursor **LFP-S** ensured complete nano-wetting of the template. The resultant material was calcined under reducing atmosphere to simultaneously preserve $LiFePO_4$ and reductively combust the carbon template. Typically, the wt% of the carbon remaining in the sample following pyrolysis and calcination was dependent on the content of EG used, the amount of residual mesoporous carbon template and the number of times the infiltration process was repeated (Table 1).

The porous morphology of the samples was probed using nitrogen adsorption techniques (Fig. 3). As shown in Table 2, the synthetic approach employed here, involving the infiltration of a porous carbon template by a novel single source precursor with calcination under a reducing atmosphere, delivered highly porous structures when compared to template free (sample 1) or the commercial $LiFePO_4$ sample. Whilst much of the porosity may be attributable to the residual carbon template, the dispersion of small $LiFePO_4$ particles throughout the porous matrix should also lead to a very high effective surface area for the active material. The $LiFePO_4$/C composites generated from the cubic mesoporous KIT-6 carbon template[41] uniformly exhibit a type IV isotherm with hysteresis, indicative of a mesoporous morphology. Employment of the single source precursor **LFP-S** (sample 3) delivers markedly enhanced surface areas in comparison to a material derived from separate Li, Fe and P sources (sample 4). As both sample 3 and 4 employed the mesoporous carbon template, the 61% increase in surface area between these samples can be attributed to improved pore infiltration and the use of the single source precursor **LFP-S**. Separate Li, Fe and P sources are more likely to form large components of bulk, non-porous $LiFePO_4$ due to the non-optimised templating chemistry. As

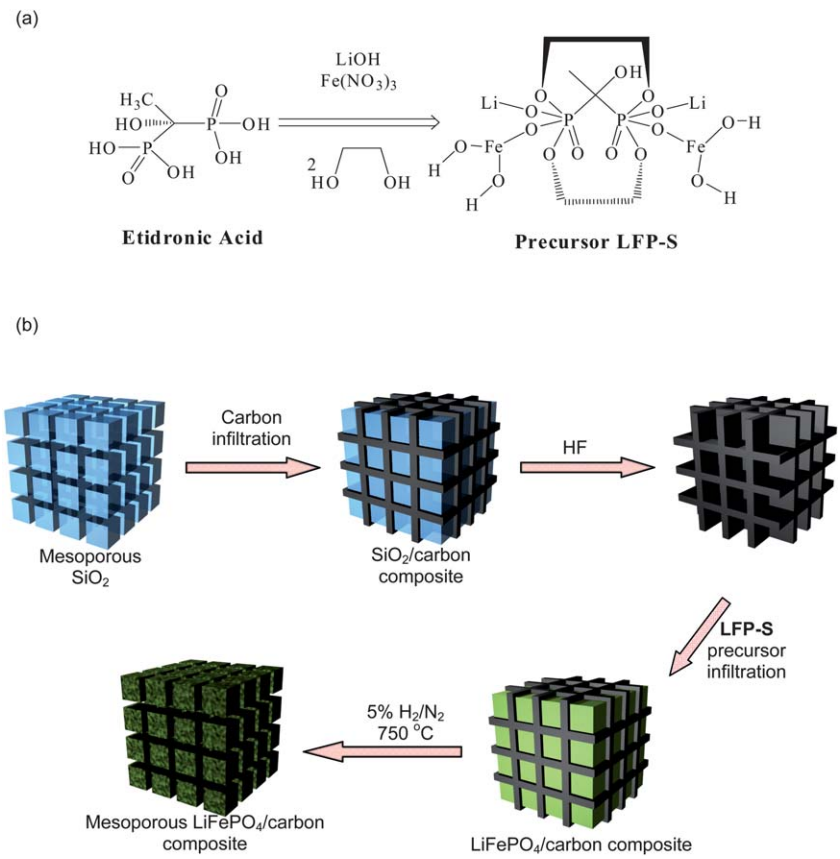

Fig. 1 (a) Synthesis and the structure of the single source precursor **LFP-S**, and (b) the novel synthetic process of a single source precursor infiltration into a hard template to give the $LiFePO_4$/carbon composite.

Table 1 Summary of $LiFePO_4$/composite samples used in the study

Sample	Precursor	Template	EG equivalents	Template precursor loading cycles	% Carbon content
1	**LFP-S**	None	3	—	6.9
2	**LFP-S**	Cubic mesoporous carbon	2	1	49.8
3	**LFP-S**	Cubic mesoporous carbon	3	1	65.6
4	Separate sources	Cubic mesoporous carbon	n/a	1	47.3
5	**LFP-S**	Cubic mesoporous carbon	3	3	36.8
6	Commercial $LiFePO_4$				1.6

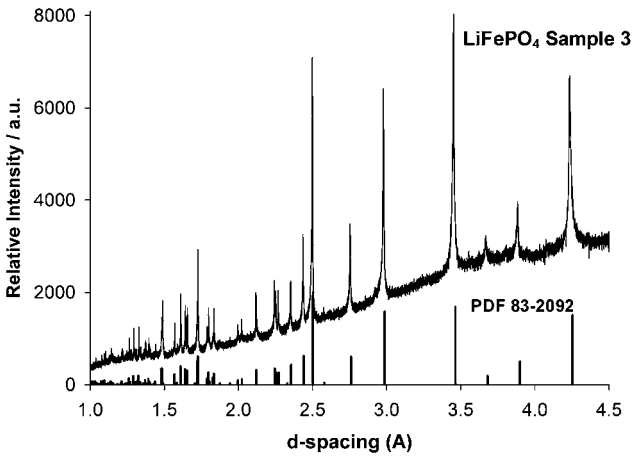

Fig. 2 Sample 3 delivers a phase pure $LiFePO_4$ within the templated carbon matrix after calcination at 750 °C. Data obtained using synchrotron radiation, $\lambda = 1.00$ Å.

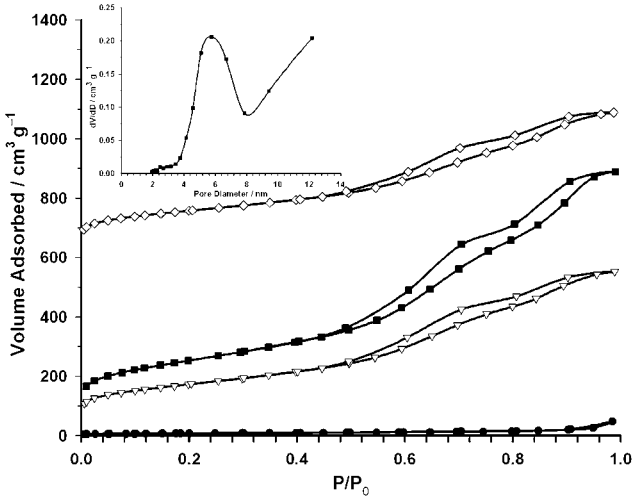

Fig. 3 Nitrogen adsorption isotherms for: sample 1 (closed circles, ●); sample 2 (open triangles, ▽); sample 3 (closed squares, ■); sample 4 (open diamonds, ◇). Sample 4 has been shifted 600 units on the *y*-axis for clarity. All other samples remain unchanged. Inset: BdB–FHH pore size distribution from the adsorption branch of BET/77 K/N_2 isotherm for 31 wt.% mesoporous $LiFePO_4$ (sample 3).

shown in Fig. 3 (inset), the composites maintained a high degree of ordered meso-porosity following partial reduction and an increase in pore size from 3.5 nm, in the carbon template, to 5–6 nm in the composite.

The TEM images shown in Fig. 4 indicate a structure where a thin, porous carbon 'skeleton' is uniformly coated by largely amorphous $LiFePO_4$, which also has smaller $LiFePO_4$ crystallites interspersed within the carbon matrix. Closer examination reveals that these particles are directly bound to the carbon matrix. Fig. 4a shows a bright-field (BF)-TEM image of a representative region of the sample. This region contains roundish, dark-contrast particles and lower-contrast, porous material. Large micron-sized particles as well as much smaller particles are clearly visible. Selected-area electron diffraction and high-resolution TEM imaging revealed that the darker contrast particles had a crystal structure consistent with that of $LiFePO_4$ (orthorhombic, space group *Pnma*, lattice parameters $a = 10.32$ Å, $b = 6.00$ Å, $c = 4.69$ Å). For example, in Fig. 4 (insets a1 and a2) the smaller particle exhibits lattice fringes with a spacing of 2.98 Å, a value very close to the inter-planar distance of 3.00 Å for the (020) planes of $LiFePO_4$ as shown in the high resolution image (inset a2). Also apparent in the high-resolution image are highly corrugated layers of graphitic carbon, in particular around $LiFePO_4$ particles. This strongly suggests that the crystalline $LiFePO_4$ particle nucleated and grew within the porous carbon matrix.

EDX chemical maps for the region framed in Fig. 4 (inset a1) and imaged by high-angle annular dark field STEM in Fig. 4b are presented in Fig. 4c–g. Lithium cannot be detected by EDX spectroscopy. However, X-ray K-shell peaks for carbon (C), iron (Fe), phosphorus (P) and oxygen (O) could be unambiguously identified and their spatial distribution reconstructed. Within a matrix of porous carbon (Fig. 4d) many fine nano-sized particles enriched in Fe, P and O can be seen (Fig. 4e–g). In particular, the two larger particles displaying dark contrast in the TEM image (Fig. 4a, inset a1) contain Fe, P and O and can thus be assigned to $LiFePO_4$ crystals. Their dark region in BF-TEM is attributable to their crystallinity and hence stronger diffraction contrast compared with the porous carbon, as well as to their higher atomic mass due to the presence of Fe; this "Z-contrast" is apparent in the HAADF-STEM image as a bright region. Several less-defined regions enriched in Fe, P and O are also visible, suggesting that nanoscopic particles are present and highly dispersed within the carbon matrix. These results confirm that the single source precursor **LFP-S** leads to highly effective infiltration of the porous carbon matrix.

The electrochemical performances and reversible Li^+ charge insertion/extraction of the mesoporous $LiFePO_4$/carbon composite were examined using galvanostatic charge–discharge techniques over the voltage range of 2.2 V to 4.0 V (*vs.* Li/Li^+). Results of the galvanostatic profile are represented in Fig. 5 and show the initial formation charging, high-rate performance and

Table 2 Summary of surface area characterisation measurements for prepared $LiFePO_4$ samples 1–4, derived from mesoporous carbon template

	Sample 1	Sample 2	Sample 3	Sample 4	Commercial $LiFePO_4$	Cubic mesoporous carbon template
BET surface area/m^2 g^{-1}	25	604	886	551	15	604
Total pore volume/cm^3 g^{-1}[a]	0.07	0.86	1.32	0.70	0.037	0.90
Average pore size/nm[b]	14.15	5.72	6.20	5.75	10.06	3.5

[a] Measured at $P/P_0 = 0.95$. [b] Determined through the application of the BdB–FHH equations[42] to the adsorption branch of the nitrogen isotherm.

stable cycling capacities of mesoporous $LiFePO_4$ (sample 3) compared to those of sample 1 (untemplated) and a commercial source of $LiFePO_4$. For ease of interpretation, the galvanostatic profile has been split into two separate charts where the top chart has the initial formation charge stage (cycles 1–5) and the extended cycling results (cycles 60–160), separated by a region of increased rate discharge cycles (intentionally blank on top chart). The results from the high rate discharging (cycles 6–59) are captured in the middle chart with an expanded cycle number axis. An excellent reversible capacity of 163 A h kg^{-1} for the mesoporous sample 3, 145 A h kg^{-1} for the commercial $LiFePO_4$ and 80 A h kg^{-1} for the untemplated sample 1 was observed. As the contribution from the residual carbon matrix is expected to be relatively low, the reported capacities are based on the weight of the active material only.[19] At these moderate charge/discharge rates (0.1 *C*/0.2 *C*) the mesoporous samples achieve almost quantitative utilization of the $LiFePO_4$ approaching its theoretical capacity (170 A h kg^{-1}) which can be attributed to the unique morphology, and molecular scale mixing of the fine active material within the conductive carbon matrix, providing greatly improved active material accessibility. As noted in the *Experimental section*, samples 2–5 which already have significant quantities of residual carbon from the templating process did not require the addition of extra (*ex situ*) conductive carbon whereas sample 1 and the commercial $LiFePO_4$ required additional carbon (typically 20%) to achieve an acceptable capacity. Whilst even higher rates of *ex situ* carbon addition did slightly increase the capacity of the non-templated samples, their capacities never reached those of the templated samples, even at similar or higher carbon loadings.

The high capacity and remarkable capacity retention of the mesoporous $LiFePO_4$ composite are further exemplified during the extended cycling (top, Fig. 5) where after 100 cycles, at 1 *C* charge and 1 *C* discharge, the reversible capacity of sample 3 is still ~155 A h kg^{-1} compared to 125 A h kg^{-1} for the commercial sample and 62 A h kg^{-1} for sample 1. There is a striking performance contrast between sample 1 (without template) and sample 3 (with carbon template), which are both prepared from the precursor **LFP-S**; which again is attributed to the intimate dissolution and dispersion of the active material, and the nanostructure directing properties of the mesoporous carbon–$LiFePO_4$ composite matrix.

Much discussion in the literature has focussed on the exceptional performance from the nanostructured $LiFePO_4$ and the rate limitations imposed by solid-state transport during the interfacial insertion/extraction process. This has also met with some controversy especially with regard to high rate performance of electrodes, for instance, the report by Kang and Ceder.[23] Of particular interest has been the discussion of the concentration gradient associated with the electrolyte and its effect as the principal rate limiting process during rapid discharge.[43] Johns *et al.* have proposed a 'sharp discharge front' associated with diffusion of ions from an ionic reservoir as the rate limiting process for rapid discharge of $LiFePO_4$ composite electrodes. In the case of the mesoporous samples we prepared for this study, this effect would be minimal due to the high porosity (which acts as an electrolyte reservoir) and the ratio of active material to porous carbon. Consideration of the structural and composition data we have presented for our mesoporous $LiFePO_4$ samples and the results of high rate discharge cycling (middle chart, Fig. 5) strongly supports this model. Presented in Fig. 5 (middle) are specific discharge capacities for triplicate cycles of 0.25 *C* charge and increasing discharge from 0.2 *C* to 23 *C* for each of sample 1, sample 3 and the commercial $LiFePO_4$ electrodes. Superior performance and exceptional resilience to rapid discharge are observed for sample 3, where its discharge capacity at 0.2 *C* = 160 A h kg^{-1} decreasing only to 128 A h kg^{-1} at 23 *C* (discharge in < 160 seconds). This result is unrivalled by the two control samples and exhibits exceptional competitive performance to recent reports of similar composite materials.[25] Although the crystalline hollow nanowire structure of Lim *et al.* demonstrates that a nanostructure in the absence of significant residual carbon can still give rise to improved utilisation.[26] This constitutes only a marginal 20% capacity loss at high discharge rates compared to 70% for the commercial $LiFePO_4$ and 73% for the untemplated sample 1, despite all samples possessing a high crystallinity and purity. This suggests that the performance is primarily related to the electrode composition, and the intimate carbon connectivity formed by the carbon matrix which also acts as a very effective electrolyte reservoir. Indeed, the superior performance afforded by the mesoporous templated material is further revealed when the corresponding specific discharge power is considered at discharge rates up to 10 *C* (bottom, Fig. 5). The intimate $LiFePO_4$–carbon composite not only affords benefits due to the reduced transport distance of Li^+ ions, the intimately bound carbon matrix displays a reduced electrode resistance that results in exceptional delivery of > 11 000 W kg^{-1} at 10 *C* for sample 3, compared to ~4000 W kg^{-1} for sample 1 and the commercial $LiFePO_4$. These results are consistent with reports by Arbizzani *et al.* for sol–gel derived $LiFePO_4$ and those of Beninati *et al.* where microwave synthesis gave rise to finely agglomerated active material and enhanced utilisation and power output.[44,45]

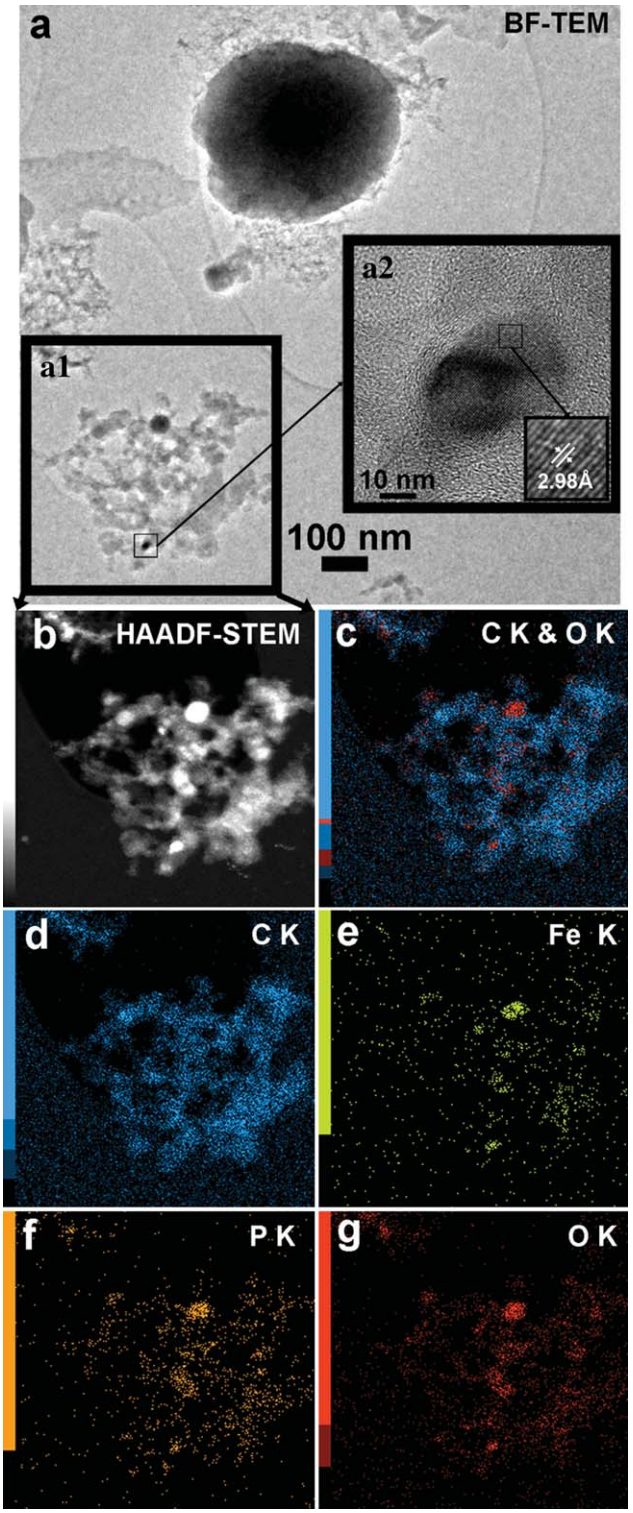

Fig. 4 (a) Bright-field (BF)-TEM image of a representative region of sample 3; (b) high-angle annular dark field (HAADF)-STEM for the region framed in (a1); EDX chemical maps from HAADF-STEM depicting X-ray K-shell peaks for: (c) carbon, C, and oxygen, O; (d) carbon, C; (e) iron, Fe; (f) potassium, P; and (g) oxygen, O.

The reversible Li^+ charge insertion/extraction of the mesoporous $LiFePO_4$/carbon composite was investigated *via* electrochemical cyclic voltammetry. Depicted in Fig. S3† is a typical

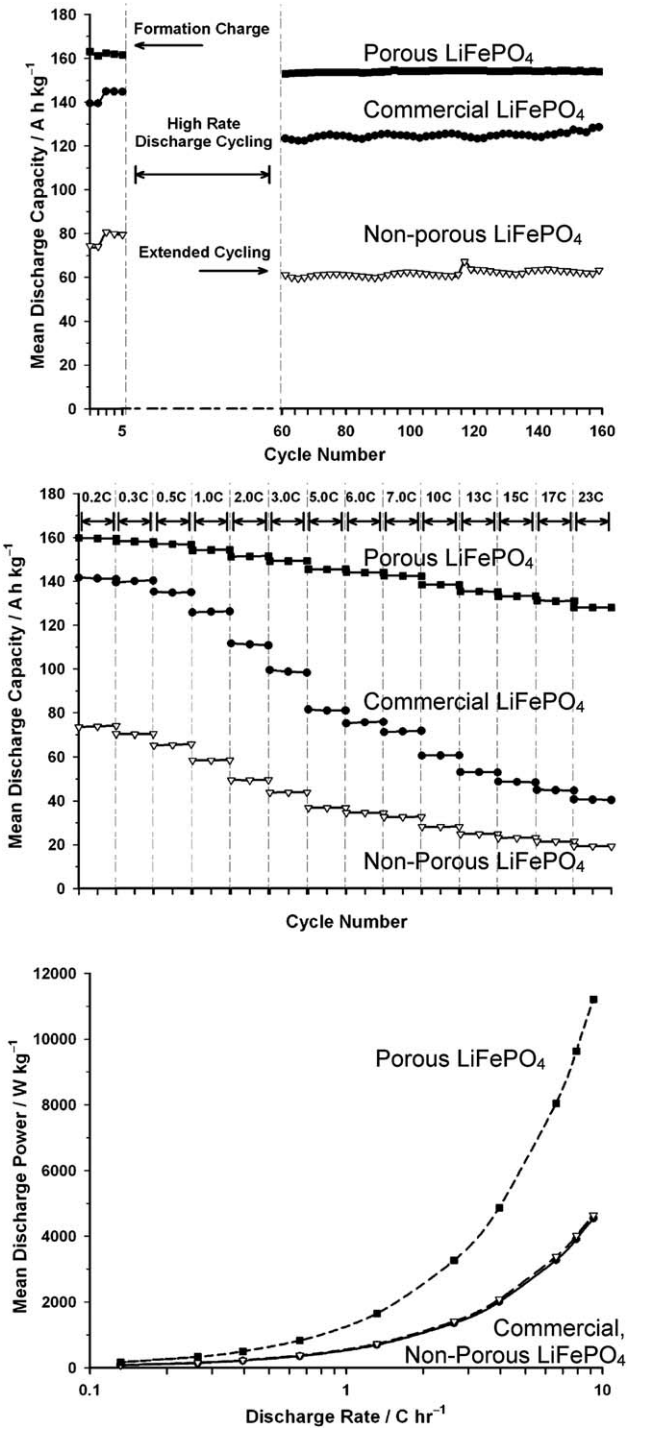

Fig. 5 (Top) Galvanostatic cycling regime of the test cells, charged at 1 *C* and discharge at 1 *C* for cycles 60–160; (middle) specific discharge capacity and as a function of cycle number and discharge rate. All cells were charged at 0.25 *C* and discharged as indicated at the top of the chart; (bottom) specific discharge capacity and mean discharge power as a function of charge rate for selected $LiFePO_4$ samples (m_{act} = sample 1, commercial sample = 2.5 ± 0.17 mg cm^{-2}, sample 3 = 1.6 ± 0.11 mg cm^{-2}) in a two-electrode CR 2032 coin cell. Commercial sample (—●—); sample 1 (---▽---) and sample 3 (---■---) as the working electrode, 1 M $LiPF_6$ (50 : 50 w/w EC : DMC) electrolyte, Li-metal anode as the secondary electrode.

transient voltammogram obtained at a 0.1 mV s^{-1} sweep of $LiFePO_4$ prepared from our precursor and labelled as untemplated $LiFePO_4$ (sample 1). A cathodic sweep in a 2-electrode cell from 2.0 V (*vs.* Li/Li^+) results in a well-defined oxidation at the reported potential (E_p^{ox}) of 3.56 V and the material exhibits a flat voltage plateau at potentials up to 4.5 V (*vs.* Li/Li^+). Excellent reversibility (Li^+ extraction) is observed during the anodic sweep where a reduction of the quasi-$FePO_4$ structure was observed at $E_p^{red} = 3.30$ V to give $E^{o\prime}$ of 3.43 V, consistent with literature reports for $LiFePO_4$ samples prepared in a similar manner.[46]

Conclusions

This work has described a novel synthetic process whereby a single molecular source precursor was developed and used to infiltrate a structured mesoporous carbon template. Pyrolytic reduction of this solid–liquid mixture gave an intimately bound dispersion of nanostructured $LiFePO_4$ clusters in stoichiometric proportions within a carbon matrix. The benefit of the composite carbon matrix, although high in carbon is the uniformly coated thin layer surrounding the $LiFePO_4$, resulting in a $LiFePO_4$/C composite exhibiting periodic, interconnected pores of 5–6 nm and an excellent active material accessibility and utilization with direct $LiFePO_4$–C bonding as a result of the single source precursor. Evaluation of the electrochemical performance, *via* cyclic voltammetry and galvanostatic charge–discharge cycling demonstrated an exceptional high rate material that displayed specific discharge capacities of 163 A h kg^{-1} (close to theoretical unity of 170 A h kg^{-1}) at 0.2 *C*, and 128 A h kg^{-1} at 23 *C* and good cyclability. The best material in this study was found to deliver almost three times the specific power of commercial $LiFePO_4$ at 10 *C*. The ease of synthetic preparation of nanostructured $LiFePO_4$/C composite together with its stable electrochemical performance shows promise for high-power energy storage applications.

Acknowledgements

This work was funded through the CSIRO Energy Transformed Flagship. Funding from the Victorian State Government for the JEOL 2100F microscope is acknowledged.

References

1 A. K. Padhi, K. S. Nanjundaswamy, C. Masquelier, S. Okada and J. B. Goodenough, *J. Electrochem. Soc.*, 1997, **144**(5), 1609.
2 H. Huang, S. C. Yin and L. F. Nazar, *Electrochem. Solid-State Lett.*, 2001, **4**(10), A170.
3 A. Yamada, S. C. Chung and K. Hinokuma, *J. Electrochem. Soc.*, 2001, **148**(3), A224.
4 G. Meligrana, C. Gerbaldi, A. Tuel, S. Bodoardo and N. Penazzi, *J. Power Sources*, 2006, **160**(1), 516.
5 A. S. Andersson, B. Kalska, L. Haggstrom and J. O. Thomas, *Solid State Ionics*, 2000, **130**(1–2), 41.
6 D. H. Kim and J. Kim, *Electrochem. Solid-State Lett.*, 2006, **9**(9), A439.
7 D. Y. W. Yu, K. Donoue, T. Inoue, M. Fujimoto and S. Fujitani, *J. Electrochem. Soc.*, 2006, **153**(5), A835.
8 S. Y. Chung, J. T. Bloking and Y. M. Chiang, *Nat. Mater.*, 2002, **1**(2), 123.
9 D. Y. Wang, H. Li, S. Q. Shi, X. J. Huang and L. Q. Chen, *Electrochim. Acta*, 2005, **50**(14), 2955.
10 N. Ravet, Y. Chouinard, J. F. Magnan, S. Besner, M. Gauthier and M. Armand, *J. Power Sources*, 2001, **97–8**, 503.
11 R. Dominko, J. M. Goupil, M. Bele, M. Gaberscek, M. Remskar, D. Hanzel and J. Jamnik, *J. Electrochem. Soc.*, 2005, **152**(5), A858.
12 Z. H. Chen, Z. H. Lu and J. R. Dahn, *J. Electrochem. Soc.*, 2002, **149**(12), A1604.
13 P. S. Herle, B. Ellis, N. Coombs and L. F. Nazar, *Nat. Mater.*, 2004, **3**(3), 147.
14 C. Delacourt, P. Poizot, S. Levasseur and C. Masquelier, *Electrochem. Solid-State Lett.*, 2006, **9**(7), A352.
15 S. B. Lee, S. H. Cho, S. J. Cho, G. J. Park, S. H. Park and Y. S. Lee, *Electrochem. Commun.*, 2008, **10**(9), 1219.
16 L. Wang, G. C. Liang, X. Q. Ou, X. K. Zhi, J. P. Zhang and J. Y. Cui, *J. Power Sources*, 2009, **189**(1), 423.
17 G. X. Wang, L. Yang, S. L. Bewlay, Y. Chen, H. K. Liu and J. H. Ahn, *J. Power Sources*, 2005, **146**(1–2), 521.
18 Z. H. Chen and J. R. Dahn, *J. Electrochem. Soc.*, 2002, **149**(9), A1184.
19 X. L. Wu, L. Y. Jiang, F. F. Cao, Y. G. Guo and L. J. Wan, *Adv. Mater.*, 2009, **21**(25–26), 2710.
20 Y. Q. Wang, B. L. Wang, J. Yang and Y. N. Nuli, *Adv. Funct. Mater.*, 2006, **16**(16), 2135.
21 C. Z. Lu, G. T. K. Fey and H. M. Kao, *J. Power Sources*, 2009, **189**(1), 155.
22 J. Liu, J. W. Wang, X. D. Yan, X. F. Zhang, G. L. Yang, A. F. Jalbout and R. S. Wang, *Electrochim. Acta*, 2009, **54**(24), 5656.
23 B. Kang and G. Ceder, *Nature*, 2009, **458**(7235), 190.
24 K. Zaghib, J. B. Goodenough, A. Mauger and C. Julien, *J. Power Sources*, 2009, **194**(2), 1021.
25 (*a*) C. M. Doherty, R. A. Caruso, B. M. Smarsly, P. Adelhelm and C. J. Drummond, *Chem. Mater.*, 2009, **21**(21), 5300; (*b*) C. M. Doherty, R. A. Caruso, B. M. Smarsly and C. J. Drummond, *Chem. Mater.*, 2009, **21**(13), 2895.
26 S. Lim, C. S. Yoon and J. Cho, *Chem. Mater.*, 2008, **20**(14), 4560–4564.
27 F. F. C. Bazito and R. M. Torresi, *J. Braz. Chem. Soc.*, 2006, **17**(4), 627.
28 M. R. Hill, J. Booth, L. Bourgeois and H. J. Whitfield, *Dalton Trans.*, 2010, **39**, 5306.
29 P. Yang, D. Zhao, D. I. Margolese, B. F. Chmelka and G. D. Stucky, *Chem. Mater.*, 1999, **11**(10), 2813.
30 T. Valdés-Solís and A. B. Fuertes, *Mater. Res. Bull.*, 2006, **41**(12), 2187.
31 R. Dominko, M. Bele, M. Gaberscek, M. Remskar, D. Hanzel, J. M. Goupil, S. Pejovnik and J. Jamnik, *J. Power Sources*, 2006, **153**(2), 274.
32 X. F. Guo, W. P. Ding, X. G. Wang and Q. J. Yan, *Chem. Commun.*, 2001, (8), 709.
33 J. Santos-Pena, P. Soudan, C. Aren, G. Palomino and S. Franger, *J. Solid State Electrochem.*, 2006, **10**(1), 1.
34 S. M. Zhu, H. S. Zhou, T. Miyoshi, M. Hibino, I. Honma and M. Ichihara, *Adv. Mater.*, 2004, **16**(22), 2012.
35 J. B. Goodenough, K. S. Nanjundaswamy, C. Masquelier, A. K. Padhi and M. Armand, *Cathode materials for rechargeable secondary lithium batteries—comprising transition metal compounds with ordered olivine or rhombohedral NASICON structure containing phosphate ions*, WO9740541-A, 1997.
36 D. Y. Zhao, B. Z. Tian and X. Y. Liu, Designer Synthesis of Mesoporous Solids *via* Block Copolymer Templating Pathway, in *Mesoporous Crystals and Related Nano-Structured Materials*, 2004, vol. 148, p. 139.
37 Y. Wan and D. Y. Zhao, *Chem. Rev.*, 2007, **107**(7), 2821.
38 Y. Meng, *Angew. Chem., Int. Ed.*, 2005, **44**(43), 7053.
39 B. F. Wang, Y. L. Qiu and L. Yang, *Electrochem. Commun.*, 2006, **8**(11), 1801.
40 S. Jun, S. H. Joo, R. Ryoo, M. Kruk, M. Jaroniec, Z. Liu, T. Ohsuna and O. Terasaki, *J. Am. Chem. Soc.*, 2000, **122**(43), 10712.
41 T. W. Kim, F. Kleitz, B. Paul and R. Ryoo, *J. Am. Chem. Soc.*, 2005, **127**(20), 7601.
42 W. W. Lukens, P. Schmidt-Winkel, D. Y. Zhao, J. L. Feng and G. D. Stucky, *Langmuir*, 1999, **15**(16), 5403.
43 P. A. Johns, M. R. Roberts, Y. Wakizaka, J. H. Sanders and J. R. Owen, *Electrochem. Commun.*, 2009, **11**(11), 2089.
44 C. Arbizzani, S. Beninati and M. Mastragostino, *J. Appl. Electrochem.*, 2010, **40**(1), 7–11.
45 S. Beninati, L. Damen and M. Mastragostino, *J. Power Sources*, 2008, **180**(2), 875–879.
46 M. R. Roberts, G. Vitins and J. R. Owen, *J. Power Sources*, 2008, **179**(2), 754.

